Front. Mech. Eng. 2020, 15(4): 645–658
https://doi.org/10.1007/s11465-020-0601-7

RESEARCH ARTICLE

Tie ZHANG, Caicheng WU, Yanbiao ZOU

Chord error constraint based integrated control strategy for contour error compensation

© Higher Education Press 2020

Abstract As the traditional cross-coupling control method cannot meet the requirements for tracking accuracy and contour control accuracy in large curvature positions, an integrated control strategy of cross-coupling contour error compensation based on chord error constraint, which consists of a cross-coupling controller and an improved position error compensator, is proposed. To reduce the contour error, a PI-type cross-coupling controller is designed, with its stability being analyzed by using the contour error transfer function. Moreover, a feed rate regulator based on the chord error constraint is proposed, which performs speed planning with the maximum feed rate allowed by the large curvature position as the constraint condition, so as to meet the requirements of large curvature positions for the chord error. Besides, an improved position error compensation method is further presented by combining the feed rate regulator with the position error compensator, which improves the tracking accuracy via the advance compensation of tracking error. The biaxial experimental results of non-uniform rational B-splines curves indicate that the proposed integrated control strategy can significantly improve the tracking and contour control accuracy in biaxial contour following tasks.

Keywords cross-coupling controller, contour error, tracking error, position error compensator, feed rate regulator

1 Introduction

In biaxial motion control tasks, the great difference in the motion characteristics of coordinate axes in the feed system may result in low contour tracking accuracy when simply using the single-axis servo control. Specific contour control techniques, such as cross-coupling control (CCC) [1,2], must be used. The basic idea of CCC is to build a real-time contour error model based on the feedback information and interpolation information of each coordinate axis, seek and establish an optimal contour error control law to compensate the contour error, thus reducing and eliminating the contour error. A common cross-coupling controller mainly consists of two parts, one is the real-time contour error estimation model and the other is the control and compensation strategy [3]. The contour error is defined as the shortest normal distance from the actual cutting position to the target reference path [4,5], as shown in Fig. 1.

Contour error estimation methods have been the focus of many scholars. For example, Koren and Lo [2] and Yang and Li [6] locally approximate the free-curve profile with an intimate circle and used McLaughlin's expansion to achieve a second-order estimation of the contour error. Shih et al. [7] adopted Taylor's second-order expansion to estimate the contour error on the premise of close circular approximation. Based on the traditional second-order method of close circular approximation, Zhao et al. [3] proposed a high-precision second-order estimation method using the Taylor's expansion of distance function. Chen et al. [8] proposed several real-time parameter-based contour error estimation algorithms, in which the backward reference point was firstly calculated by means of the arc length parameter-based method, and was then used as the required command point to estimate the contour error by using the straight-line or arc approximation method.

Based on the real-time estimation of contour error, some researchers developed a variety of control schemes to reduce and eliminate the contour error. For example, Koren [1] proposed a CCC structure to compensate the contour error in biaxial contour following tasks. To improve the contour control accuracy of a system, Yan et al. [9] proposed a self-correcting adaptive control strategy based on the CCC structure and the CCC of axial motion. Based on the adaptive control method, Chen et al. [10] proposed a robust adaptive CCC strategy. Srinivasan and Kulkarni

Received March 30, 2020; accepted July 9, 2020

Tie ZHANG (✉), Caicheng WU, Yanbiao ZOU
School of Mechanical and Automotive Engineering, South China University of Technology, Guangzhou 510641, China
E-mail: merobot@scut.edu.cn

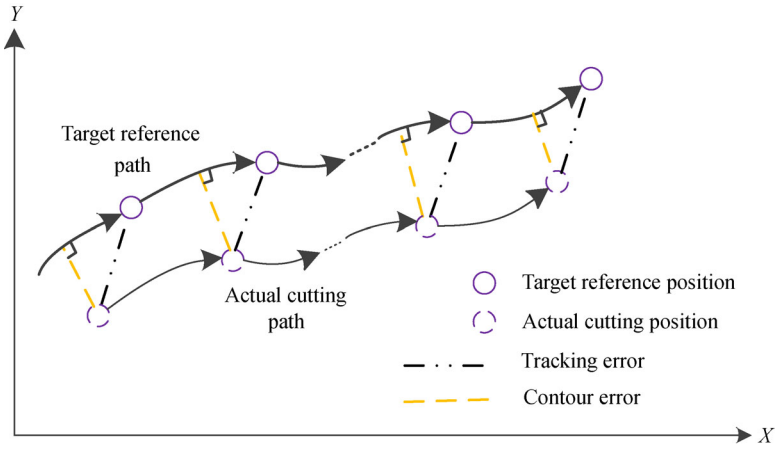

Fig. 1 Schematic of tracking and contour errors.

[11] and Ouyang et al. [12] combined the CCC structure with the proportion-integration-differentiation (PID) control algorithm to improve the contour control accuracy. Considering the limitations of the traditional CCC structure, Shin et al. [7] proposed an improved CCC structure for modifying the reference position command of each coordinate axis and designed a cross-coupling controller for contour error compensation, which can improve the contour control accuracy of biaxial contour-following tasks to a certain extent. Moreover, Chen et al. [13] designed a cross-coupling position command shaping controller for multi-axis contour following tasks based on an improved CCC structure. All these above-mentioned methods can be classified into CCC methods.

However, CCC methods cannot significantly reduce the tracking error. Poor tracking performance is likely to cause severe processing errors. To solve this problem, some researchers proposed a variety of methods for improving the contour following accuracy. For example, Su and Cheng [5] proposed a position error compensator (PEC) to improve the tracking and contour control accuracy of the biaxial motion control system. Sun et al. [14] proposed a new model-reference adaptive control strategy for improving the tracking performance. El Khalick and Uchiyama [15] proposed a model predictive contouring controller to further reduce the tracking error. Wu et al. [16] added a feedforward controller to the general-purpose cascaded P-PI feedback control structure to improve the tracking accuracy. Based on the feedforward control strategy, Cheng et al. [17] and Chen et al. [18] combined the CCC method with the feedforward control scheme to indirectly reduce the contour error by improving the tracking performance of each axis. To simultaneously reduce the tracking and contour errors, Moghadam et al. [19] combined the robust tracking with the optimal hierarchical control techniques. Based on the adaptive feed rate adjusting method, Tang and Landers [20] presented a predictive contour control strategy. Rahaman et al. [21] combined the interpolation method, CCC method and tracking controller, and further proposed a new approach to realize the simultaneous compensation of contour error and tracking error. In addition, Barton and Alleyne [22] and Tsai et al. [23] used iterative learning control method to decrease the tracking error and contour error. All these above-mentioned methods can be regarded as a combination of the CCC method and the tracking error compensation strategy.

In summary, in most cases, CCC methods are effective in reducing the contour error but ineffective in reducing the tracking error and the chord error. A combination between CCC methods and tracking error compensation strategies can improve the tracking accuracy and the contour control accuracy at the same time. However, in the process of designing the CCC controllers, many researchers did not take into account the effect of an added controller on the stability of the biaxial servo system, nor did they consider the requirements for the chord error in the large curvature position of the reference path.

To solve these problems, this paper first proposes a feed rate regulator based on the chord error constraint to meet the requirements of the large curvature position for the chord error. Then, based on the improved CCC structure proposed by Shin et al. [7], a cross-coupling controller is designed, with its stability being analyzed, so as to reduce the contour error and improve the contour control accuracy. Moreover, by combining the PEC proposed by Su and Cheng [5] with the feed rate regulator, an improved position error compensation method is proposed, which can further reduce the tracking error and improve the tracking accuracy while meeting the requirements of the large curvature position for the chord error. Besides, to achieve higher contour control accuracy, an integrated control strategy for contour error compensation, which consists of a cross-coupling controller and an improved position error compensation method, is finally proposed.

The integrated control strategy proposed in this paper

only needs to use the position and velocity information of the interpolation point as well as the curvature and chord error information of the target trajectory. This information is available in multi-axis computer numerical control (CNC) platform, so that we can use the methods such as the high-precision three-axis contour error estimation algorithm [24] and the five-axis contour error estimation algorithm [25,26] to estimate the contour error of the multi-axis CNC platform and implement the contour error compensation of each axis. Through the proposed integrated control strategy, the error compensation can be distributed to each axis, so that the tracking and contour control accuracy of the multi-axis CNC platform can be significantly improved and the chord error requirements can be successfully met. Thus, it is feasible to extend the integrated control strategy proposed in this paper to multi-axis CNC machining, which is also the focus of our future work.

2 Feed rate regulator based on chord error constraint

To solve the problem that the traditional CCC method cannot meet the chord error requirement in large curvature positions, this paper takes the non-uniform rational B-splines (NURBS) curve as the object and proposes a feed rate regulator based on the chord error constraint. The regulator is combined with the CCC strategy to meet the requirements of the large curvature position for chord error and to reduce the contour error effectively.

The schematic of chord error is illustrated in Fig. 2, where $P(u_i)$ and $P(u_{i+1})$ respectively represent the ith and $(i+1)$th interpolation points and are generated by the NURBS curve interpolator [27]. In addition, ER_i is defined as the chord error, ρ_i is the radius of curvature at the NURBS curve $u = u_i$, and L_i is the chord length for the ith interpolation period.

From Fig. 2, the chord error can be expressed as

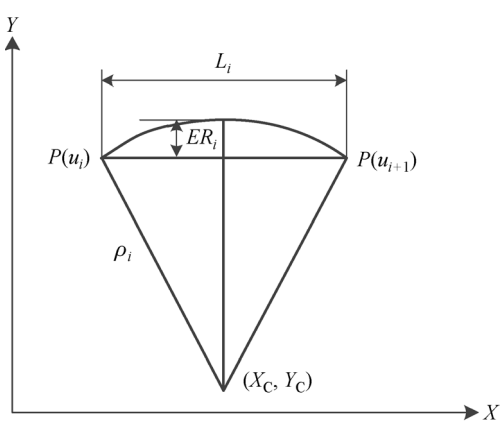

Fig. 2 Schematic of chord error.

$$ER_i = \rho_i - \sqrt{\rho_i^2 - \left(\frac{L_i}{2}\right)^2}. \quad (1)$$

Recording the maximum chord error allowed for machining as $ER_{\max}$, which satisfies $L_i = V_{\max}T_s$ where $V_{\max}$ is the maximum interpolation speed, and T_s is the sampling period. Then, the maximum interpolation speed $V_{\max}$ based on the chord error constraint in any period can be calculated as

$$\begin{aligned} V_{\max} &= \frac{2}{T_s}\sqrt{\rho_i^2 - (\rho_i - ER_{\max})^2} \\ &= \frac{2}{T_s}\sqrt{2\rho_i ER_{\max} - ER_{\max}^2}. \end{aligned} \quad (2)$$

Since the curvatures in different positions of the NURBS curve are different, the maximum feed rates allowed in different positions are also different under the constraint of chord error. Large chord error tends to occur in the position with a large curvature. Based on the chord error constraint, first, set B corresponding to all curvature maxima points is searched in set A of the entire curve interpolation points. Then, set C corresponding to the point at which the allowed maximum feed rate is smaller than the initial one (the initial feed rate is constant) is found in set B. Finally, the quintic polynomial speed planning is performed with the maximum allowable feed rate as a constraint.

The design process of the feed rate regulator is as follows:

1) Traversing the whole trajectory, find all curvature maxima points in the interpolation point set $\{P(u_1), P(u_2), ..., P(u_t)\}$, and record this set as $\{P(u_1), P(u_2), ..., P(u_n)\}$, where $t > n$.

2) Assuming that the initial feed rate is V_{start}, find the point at which the maximum feed rate $V_{\max}$ based on the chord error is smaller than the initial feed rate V_{start} in the curvature maxima point set $\{P(u_1), P(u_2), ..., P(u_n)\}$, and record this set as $\{P(u_1), P(u_2), ..., P(u_m)\}$. The maximum feed rate set allowed for each point is $\{V_{s1}, V_{s2}, ..., V_{sm}\}$, and the parameter set of the corresponding curves of each point is $\{u_{s1}, u_{s2}, ..., u_{sm}\}$, where $n > m$.

3) Assuming that curve parameter $u \in [0, 1]$, then the parameter set $\{u_{s1}, u_{s2}, ..., u_{sm}\}$ divides the curve into $(m+1)$ intervals. The intervals respectively correspond to $[0, u_{s1}], [u_{s1}, u_{s2}], ..., [u_{sm}, 1]$. Performing the speed planning with a quintic polynomial in each interval, and the starting and ending speed of each interval corresponds to $[V_{\text{start}}, V_{s1}], [V_{s1}, V_{s2}], ..., [V_{sm}, V_{\text{end}}]$.

The schematic of the speed of each interval after the planning is illustrated in Fig. 3.

4) According to the law of the quintic polynomial, the function between the feed rate $V(u)$ and the curve parameter u can be expressed as

$$V(u) = a_0 + a_1 u + a_2 u^2 + a_3 u^3 + a_4 u^4 + a_5 u^5. \quad (3)$$

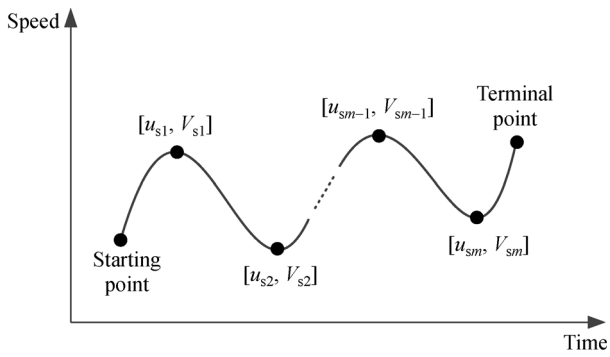

Fig. 3 Schematic of speed interval.

Thus, acceleration $A(u)$ and jerk (the change rate of acceleration) $J(u)$ can be respectively expressed as

$$A(u) = a_1 + 2a_2u + 3a_3u^2 + 4a_4u^3 + 5a_5u^4, \quad (4)$$

$$J(u) = 2a_2 + 6a_3u + 12a_4u^2 + 20a_5u^3. \quad (5)$$

Within each parameter interval $[u_s, u_e]$, in order to ensure the continuity of acceleration and jerk, boundary conditions are applied to the feed rate, acceleration and jerk to determine the coefficients of Eq. (3), which are expressed as

$$\begin{cases} a_0 + a_1u_s + a_2{u_s}^2 + a_3{u_s}^3 + a_4{u_s}^4 + a_5{u_s}^5 = v_s, \\ a_0 + a_1u_e + a_2{u_e}^2 + a_3{u_e}^3 + a_4{u_e}^4 + a_5{u_e}^5 = v_e, \\ a_1 + 2a_2u_s + 3a_3{u_s}^2 + 4a_4{u_s}^3 + 5a_5{u_s}^4 = a_s, \\ a_1 + 2a_2u_e + 3a_3{u_e}^2 + 4a_4{u_e}^3 + 5a_5{u_e}^4 = a_e, \\ 2a_2 + 6a_3u_s + 12a_4{u_s}^2 + 20a_5{u_s}^3 = J_s, \\ 2a_2 + 6a_3u_e + 12a_4{u_e}^2 + 20a_5{u_e}^3 = J_e, \end{cases} \quad (6)$$

where v_s, a_s, and J_s represent the starting velocity, acceleration and jerk of each parameter interval, respectively, and v_e, a_e, and J_e represent the end velocity, acceleration, and jerk of each parameter interval, respectively. In this paper, we set $a_s = a_e = J_s = J_e = 0$ to design the feed rate regulator.

Then, the feed rate at each interpolation point of the curve is

$$V_i = V(u_i), \quad (7)$$

where u_i is the curve parameter corresponding to each interpolation point.

3 Cross-coupling control strategy

CCC is the main method to improve the accuracy of biaxial contour following tasks. In this section, a cross-coupling controller for contour error compensation is designed based on the improved CCC structure, with its stability being analyzed by using the contour error transfer function (CETF).

3.1 Design of the cross-coupling controller

The structure of the cross-coupling controller of a biaxial servo system is illustrated in Fig. 4. In Fig. 4, R_x and R_y are reference position commands of X- and Y-axis generated by the NURBS curve interpolator, representing the position information of each interpolation point; K_{px} and K_{py} are the position loop feedback controllers in X- and Y-axis of the servo system; G_{vx} and G_{vy} are the links of X- and Y-axis, respectively, including velocity loop, current loop, and actuator, which can be obtained by model identification; P_x and P_y are the actual positions of motor output from X- and Y-axis, which can be obtained by

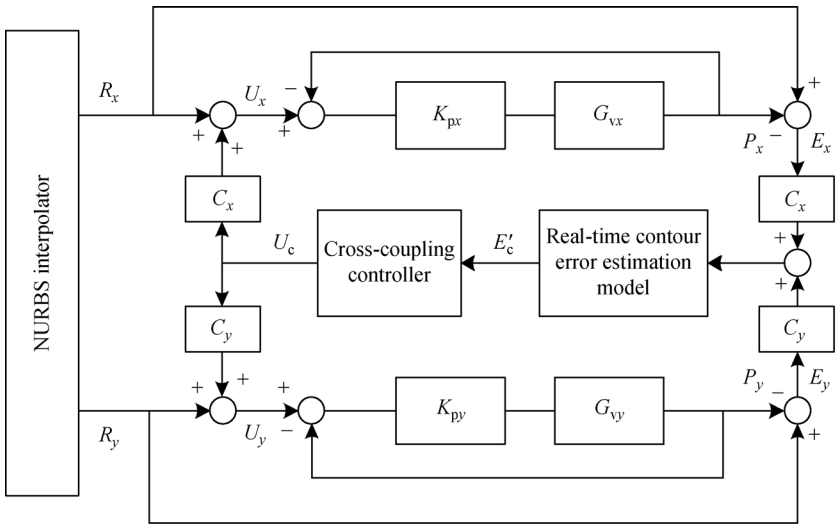

Fig. 4 Structure of cross-coupling controller for biaxial servo system.

sampling the signal of photoelectric encoder; E_x and E_y are the components of current tracking error in X- and Y-axis, respectively; C_x and C_y are the cross-coupling coefficients in X- and Y-axis of the CCC controller; and E'_c is the contour error estimated in real-time, which can be written as

$$E'_c = E_x C_x + E_y C_y. \tag{8}$$

From Fig. 4, the control inputs can be expressed as

$$U_x = R_x + U_c C_x, \tag{9}$$

$$U_y = R_y + U_c C_y, \tag{10}$$

where U_c represents the output of the estimated contour error E'_c after being acted upon by the CCC controller, and U_x and U_y are the control inputs for X- and Y-axis including reference position commands and contour error compensations.

By inputting U_x and U_y obtained in real time as reference position instructions for each sampling period into the biaxial servo system, the compensation of the cross-coupling contour error can be implemented.

The position loop feedback controllers in Fig. 4 are P-type, and the CCC controller $C_c(z^{-1})$ is designed as PI-type, with a representation in the discrete domain as

$$C_c(z^{-1}) = K_{cp} + K_{ci}\frac{1}{1-z^{-1}}, \tag{11}$$

where K_{cp} and K_{ci} are the proportional and integral gains of the CCC controller, respectively, and z is a complex variable called a Z-transform operator.

3.2 Stability analysis

The cascade control structure [13] of single-axis object in a servo system is illustrated in Fig. 5, where K_{pi} represents the position proportional gain of each axis, K_{vpi} represents the velocity proportional gain of each axis, K_{vvi} represents the velocity integral gain of each axis, $G_{pi}(z^{-1})$ represents a discrete model of single-axis object of the servo system, G_{vi} represents the link including the velocity loop and the integrator (shown by the dotted line in Fig. 5), and $i = x$ and y.

To better analyze the stability of the servo control system, the biaxial motion control system without CCC strategy (abbreviated as the uncoupled system) is equivalent to the form shown in Fig. 6, and the corresponding terms are listed in Table 1.

From Fig. 6, the transfer function matrix between the reference input and the actual output can be derived as

$$\boldsymbol{T} = \boldsymbol{K}_p \boldsymbol{G}_v (\boldsymbol{I} + \boldsymbol{K}_p \boldsymbol{G}_v)^{-1}. \tag{12}$$

Thus, the tracking error can be expressed as

$$\boldsymbol{E} = \boldsymbol{R} - \boldsymbol{P} = (\boldsymbol{I} - \boldsymbol{T})\boldsymbol{R} = (\boldsymbol{I} - \boldsymbol{K}_p \boldsymbol{G}_v (\boldsymbol{I} + \boldsymbol{K}_p \boldsymbol{G}_v)^{-1})\boldsymbol{R}. \tag{13}$$

Define the contour error (ε_u) of the uncoupled system as

$$\varepsilon_u = \boldsymbol{C}^T \cdot \boldsymbol{E} = \boldsymbol{C}^T \cdot (\boldsymbol{I} - \boldsymbol{K}_p \boldsymbol{G}_v (\boldsymbol{I} + \boldsymbol{K}_p \boldsymbol{G}_v)^{-1})\boldsymbol{R}. \tag{14}$$

The cross-coupling position command shaping controller $\boldsymbol{C}^T C_c \boldsymbol{C}$ couples the two axes together and the controller forms extra loops for modifying the reference position command for each axis. The coupled motion control system can be equivalent to the form shown in Fig. 7.

It can be seen from Fig. 7 that the control input of the coupled system is the sum of the target command position and the contour error compensations, so that the modified target command position can be expressed as

$$\boldsymbol{U} = \boldsymbol{R} + \boldsymbol{C} C_c \varepsilon_c. \tag{15}$$

Then, the following equations can be easily obtained from Fig. 7:

$$\boldsymbol{P} = \boldsymbol{U} \cdot \boldsymbol{T} = (\boldsymbol{I} + \boldsymbol{T} \cdot \boldsymbol{C} C_c \boldsymbol{C}^T)^{-1} \cdot (\boldsymbol{T} + \boldsymbol{T} \cdot \boldsymbol{C} C_c \boldsymbol{C}^T)\boldsymbol{R}, \tag{16}$$

$$\boldsymbol{E} = \boldsymbol{R} - \boldsymbol{P} = (\boldsymbol{I} + \boldsymbol{T} \cdot \boldsymbol{C} C_c \boldsymbol{C}^T)^{-1} \cdot (\boldsymbol{I} - \boldsymbol{T})\boldsymbol{R}. \tag{17}$$

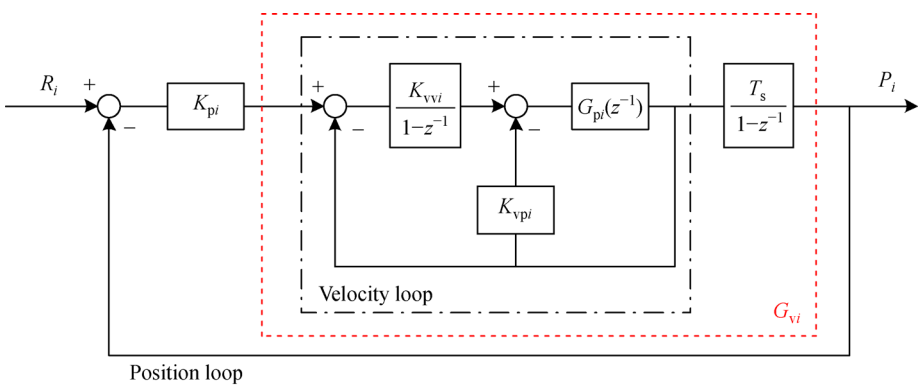

Fig. 5 Cascade control structure of single-axis object in a servo system.

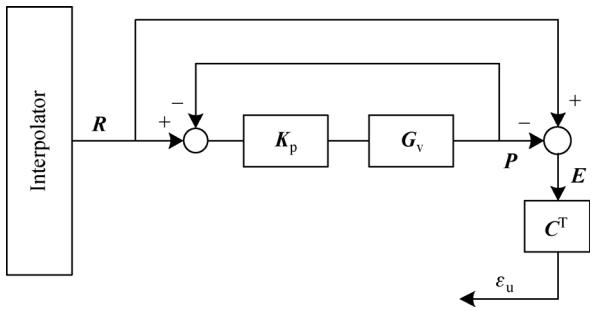

Fig. 6 Uncoupled motion control system.

Table 1 Corresponding terms in the block diagram

Corresponding term	Definition
$\boldsymbol{R} = [R_x\ R_y]^{\mathrm{T}}$	Target command position
$\boldsymbol{P} = [P_x\ P_y]^{\mathrm{T}}$	Actual cutting position
$\boldsymbol{U} = [U_x\ U_y]^{\mathrm{T}}$	Modified target command position
$\boldsymbol{E} = [E_x\ E_y]^{\mathrm{T}}$	Tracking error
$\boldsymbol{K}_{\mathrm{p}} = diag\{K_{\mathrm{p}x}\ K_{\mathrm{p}y}\}$	Position loop feedback controller
$\boldsymbol{G}_{\mathrm{v}} = diag\{G_{\mathrm{v}x}\ G_{\mathrm{v}y}\}$	Equivalent link including velocity loop and integrator
$\boldsymbol{C} = [C_x\ C_y]^{\mathrm{T}}$	Cross-coupling coefficients of CCC controller

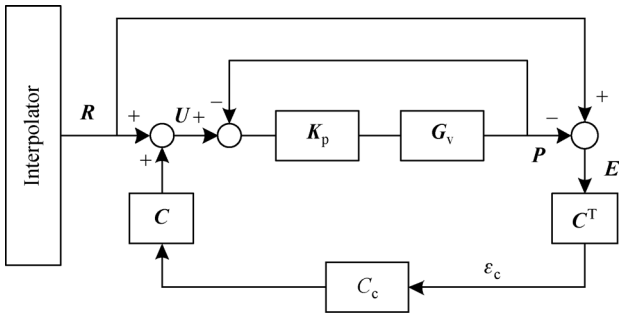

Fig. 7 Coupled motion control system.

Similarly, the contour error (ε_{c}) of the coupled system can be defined as

$$\begin{aligned}\varepsilon_{\mathrm{c}} &= \boldsymbol{C}^{\mathrm{T}}\cdot\boldsymbol{E} = \boldsymbol{C}^{\mathrm{T}}\cdot(\boldsymbol{I}+\boldsymbol{T}\cdot\boldsymbol{C}C_{\mathrm{c}}\boldsymbol{C}^{\mathrm{T}})^{-1}\cdot(\boldsymbol{I}-\boldsymbol{T})\boldsymbol{R}\\ &= \boldsymbol{C}^{\mathrm{T}}\cdot(\boldsymbol{I}+\boldsymbol{K}_{\mathrm{p}}\boldsymbol{G}_{\mathrm{v}}(\boldsymbol{I}+\boldsymbol{K}_{\mathrm{p}}\boldsymbol{G}_{\mathrm{v}})^{-1}\cdot\boldsymbol{C}C_{\mathrm{c}}\boldsymbol{C}^{\mathrm{T}})^{-1}\\ &\quad\cdot(\boldsymbol{I}-\boldsymbol{K}_{\mathrm{p}}\boldsymbol{G}_{\mathrm{v}}(\boldsymbol{I}+\boldsymbol{K}_{\mathrm{p}}\boldsymbol{G}_{\mathrm{v}})^{-1})\boldsymbol{R}.\end{aligned}\tag{18}$$

According to the matrix inversion formulas applied in Ref. [13], we can transform Eq. (18) into Eq. (19), i.e.,

$$\begin{aligned}\varepsilon_{\mathrm{c}} &= (1+\boldsymbol{C}^{\mathrm{T}}\boldsymbol{K}_{\mathrm{p}}\boldsymbol{G}_{\mathrm{v}}(\boldsymbol{I}+\boldsymbol{K}_{\mathrm{p}}\boldsymbol{G}_{\mathrm{v}})^{-1}C_{\mathrm{c}}\boldsymbol{C})^{-1}\cdot\boldsymbol{C}^{\mathrm{T}}\\ &\quad\cdot(\boldsymbol{I}-\boldsymbol{K}_{\mathrm{p}}\boldsymbol{G}_{\mathrm{v}}(\boldsymbol{I}+\boldsymbol{K}_{\mathrm{p}}\boldsymbol{G}_{\mathrm{v}})^{-1})\boldsymbol{R}.\end{aligned}\tag{19}$$

Comparing Eqs. (14) and (19), the relationship between the contour error of the coupled and the uncoupled system can be expressed as

$$\varepsilon_{\mathrm{c}} = (1+\boldsymbol{C}^{\mathrm{T}}\boldsymbol{K}_{\mathrm{p}}\boldsymbol{G}_{\mathrm{v}}(\boldsymbol{I}+\boldsymbol{K}_{\mathrm{p}}\boldsymbol{G}_{\mathrm{v}})^{-1}C_{\mathrm{c}}\boldsymbol{C})^{-1}\varepsilon_{\mathrm{u}}.\tag{20}$$

Furthermore, we can express Eq. (20) into the form of Eq. (21), that is,

$$\varepsilon_{\mathrm{c}} = \frac{1}{1+PC_{\mathrm{c}}}\varepsilon_{\mathrm{u}},\tag{21}$$

where $\dfrac{1}{1+PC_{\mathrm{c}}}$ is defined as the CETF [28], and satisfies

$$P = \boldsymbol{C}^{\mathrm{T}}\boldsymbol{K}_{\mathrm{p}}\boldsymbol{G}_{\mathrm{v}}(\boldsymbol{I}+\boldsymbol{K}_{\mathrm{p}}\boldsymbol{G}_{\mathrm{v}})^{-1}\boldsymbol{C}.\tag{22}$$

Due to the gain parameters K_{cp} and K_{ci} of the cross-coupling controller will not change in the process of tracking a target trajectory, the coupled system can be treated as a time-invariant system and the relevant theories of the CETF can be used for stability analysis. Since the controllers of the position and velocity loops of each axis use the same gain, we may consider that the two axes have almost matched dynamics. Then, the equivalent link of position proportional gain of each axis can be expressed as K_{equ}, and the equivalent link of velocity loop and integrator of each axis can be expressed as G_{equ}, i.e.,

$$K_{\mathrm{p}x} = K_{\mathrm{p}y} = K_{\mathrm{equ}},\tag{23}$$

$$G_{\mathrm{v}x} = G_{\mathrm{v}y} = G_{\mathrm{equ.}}\tag{24}$$

According to the third-order contour error estimation method described in Ref. [24], the contour error of the free path can be expressed as

$$E_{\mathrm{c}}' = \boldsymbol{r}_{\mathrm{ap}}(s_0,\ \delta_s)-\boldsymbol{P},\tag{25}$$

where E_{c}' is defined as the estimated contour error, $\boldsymbol{r}_{\mathrm{ap}}$ is the approximated desired contour, δ_s is defined as $\delta_s = s-s_0$ and s is the arc length parameter, while s_0 is the arc length parameter corresponding to the target command position, and $\boldsymbol{P}$ is the actual cutting position corresponding to the target command position.

According to the geometric relationship among the target command position $\boldsymbol{R}$, the actual cutting position $\boldsymbol{P}$ and the point $\boldsymbol{r}_{\mathrm{ap}}(s_0,\ \delta_s)$ on the approximated desired contour obtained by analytical solution, we can rewrite Eq. (25) in the form of Eq. (8). In Eq. (8), E_x and E_y are respectively the components of current tracking error in X- and Y-axis, and satisfy

$$E_x = R_x-P_x,\tag{26}$$

$$E_y = R_y-P_y.\tag{27}$$

To facilitate the stability analysis of the cross-coupling controller using the CETF, we can approximate $\boldsymbol{C}^{\mathrm{T}}\cdot\boldsymbol{C}$ in

Eq. (22) to 1. Thus, Eq. (22) can be simplified into

$$P = \frac{K_{\text{equ}} G_{\text{equ}}}{1 + K_{\text{equ}} G_{\text{equ}}}. \tag{28}$$

Therefore, the complex relationship between the coupled and the uncoupled systems could be simplified as a single input-single output problem shown in Fig. 8. According to the rule of cascade control, once the controllers of velocity loop in Fig. 5 are tuned appropriately (i.e., the bandwidth of velocity loop is at least three times larger than that of the position loop, and the step response behaves no oscillation), the velocity loop can be simplified as a unit gain [7].

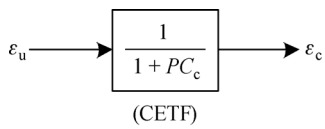

Fig. 8 Equivalent system of the contour error transfer function (CETF).

At this time, according to Eq. (24) and Fig. 5, G_{equ} can be written as $G_{\text{equ}} = \frac{T_s}{1-z^{-1}}$. Then, according to Eq. (28), $P(z^{-1})$ can be expressed as

$$P(z^{-1}) = \frac{K_{\text{equ}} T_s}{(1 + K_{\text{equ}} T_s) - z^{-1}}. \tag{29}$$

As described in Ref. [7], the system is stable when the biaxial motion control system satisfies the following conditions: Condition 1: The individual axial tracking system is stable; Condition 2: CETF is stable. Since the single-axis object of the servo system is a single input-single output system with cascade control, the actual output can track the reference input well. Therefore, Condition 1 is satisfied. While for Condition 2, according to Eqs. (11), (21), and (29), the characteristic equation of the CETF can be written as

$$D(z) = z^2 - \frac{2 + K_{\text{equ}} T_s + K_{\text{equ}} T_s K_{\text{cp}}}{1 + K_{\text{equ}} T_s + K_{\text{equ}} T_s K_{\text{cp}} + K_{\text{equ}} T_s K_{\text{ci}}} z + \frac{1}{1 + K_{\text{equ}} T_s + K_{\text{equ}} T_s K_{\text{cp}} + K_{\text{equ}} T_s K_{\text{ci}}} = 0. \tag{30}$$

By making a z–ω transformation of Eq. (30) and letting $z = \frac{\omega + 1}{\omega - 1}$, the characteristic equation of the ω-domain can be expressed as

$$D(\omega) = (a + b + 1)\omega^2 + (2a - 2)\omega + (a - b + 1) = 0, \tag{31}$$

where $a = 1 + K_{\text{equ}} T_s + K_{\text{equ}} T_s K_{\text{cp}} + K_{\text{equ}} T_s K_{\text{ci}}$, and $b = -(2 + K_{\text{equ}} T_s + K_{\text{equ}} T_s K_{\text{cp}})$.

Then, by writing the Routh table according to Eq. (31) and using the Routh stability criterion, the ranges of gains K_{cp} and K_{ci} of the cross-coupling controller satisfying the conditions can be expressed as

$$K_{\text{cp}} + K_{\text{ci}} > -1, \tag{32}$$

$$K_{\text{ci}} > 0, \tag{33}$$

$$2K_{\text{cp}} + K_{\text{ci}} > \frac{-4 - 2K_{\text{equ}} T_s}{K_{\text{equ}} T_s}. \tag{34}$$

4 Integrated motion control scheme

Since the target trajectory of a biaxial contour following task is often a free curve with variable curvatures, it is necessary to meet the chord error requirement in high-precision cases. To meet the requirement of chord error and further improve the tracking and contour control accuracy of the biaxial motion control system, an integrated control strategy with cross-coupling contour error compensation, which consists of a cross-coupling controller and an improved PEC, is proposed. In this strategy, a PI-type cross-coupling controller is designed to reduce the contour error, based on which an improved PEC is proposed to utilize real-time estimated contour error information and the speed being planned by the feed rate regulator to calculate the tracking error compensation margin. The compensation margin is taken as part of the system control input, so that the tracking error can be compensated in advance.

4.1 Improved position error compensation strategy

Since CCC methods cannot significantly reduce the tracking error, and poor tracking performance is likely to cause serious processing errors, here we combine the PEC proposed in Ref. [5] with the feed rate regulator proposed in Section 2 to further propose an improved position error compensation method. The principle of the improved compensator is shown in Fig. 9.

The design process of the improved PEC is as follows:

1) Firstly, a feed rate regulator based on chord error constraint is used to plan the speed so that the two axes can move according to the designed speed law.

2) Next, the moving coordinate system XPY is established with the actual cutting position as the origin. Assuming that each contour error can be eliminated in one sampling period when the CCC structure is used, there obtains the compensation speed $\boldsymbol{V}_c$ along the contour error direction as

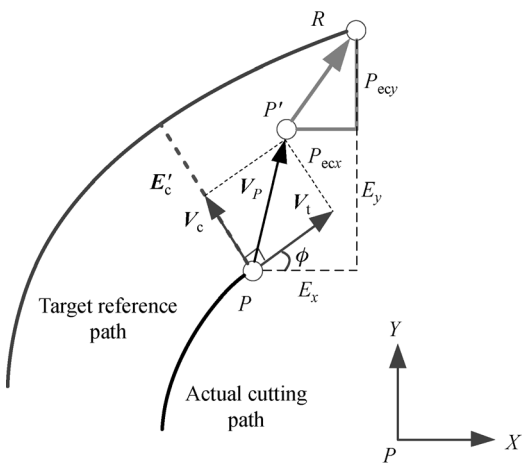

Fig. 9 Schematic of the improved position error compensator.

$$\boldsymbol{V}_{\mathrm{c}} = \frac{\boldsymbol{E}'_{\mathrm{c}}}{T_{\mathrm{s}}} = V_{\mathrm{c}x}\boldsymbol{i} + V_{\mathrm{c}y}\boldsymbol{j}, \tag{35}$$

where $\boldsymbol{E}'_{\mathrm{c}}$ is the contour error vector, T_{s} is the sampling period, and $\boldsymbol{V}_{\mathrm{c}x}$ and $\boldsymbol{V}_{\mathrm{c}y}$ are the components of the compensation speed $\boldsymbol{V}_{\mathrm{c}}$ in X- and Y-axis, respectively.

3) Then, the feed rate $\boldsymbol{V}_{\mathrm{t}}$ at the current moment at Point P can be expressed as

$$\boldsymbol{V}_{\mathrm{t}} = V_{Px}\boldsymbol{i} + V_{Py}\boldsymbol{j}, \tag{36}$$

where V_{Px} and V_{Py} are the components of the feed rate at Point P in X- and Y-axis, respectively.

4) According to the compensation speed $\boldsymbol{V}_{\mathrm{c}}$ and the feed rate $\boldsymbol{V}_{\mathrm{t}}$ at the current time, the composite speed $\boldsymbol{V}_P$ at Point P can be calculated as

$$\boldsymbol{V}_P = \boldsymbol{V}_{\mathrm{t}} + \boldsymbol{V}_{\mathrm{c}} = (V_{Px} + V_{\mathrm{c}x})\boldsymbol{i} + (V_{Py} + V_{\mathrm{c}y})\boldsymbol{j}. \tag{37}$$

5) According to the composite speed $\boldsymbol{V}_P$, the position P' after the moving for one sampling period can be calculated, and the corresponding position vector can be expressed as

$$\boldsymbol{P}' = (V_{Px} + V_{\mathrm{c}x})T_{\mathrm{s}}\boldsymbol{i} + (V_{Py} + V_{\mathrm{c}y})T_{\mathrm{s}}\boldsymbol{j}. \tag{38}$$

6) Representing the position vector of the target command position R in the XPY coordinate system as

$$\boldsymbol{R} = E_x\boldsymbol{i} + E_y\boldsymbol{j}, \tag{39}$$

where E_x and E_y are respectively the components of current tracking error in X- and Y-axis, and can be obtained by Eqs. (26) and (27).

Thus, the distance vector between P' and R can be expressed as

$$\boldsymbol{P'R} = [E_x - (V_{Px} + V_{\mathrm{c}x})T_{\mathrm{s}}]\boldsymbol{i} + [E_y - (V_{Py} + V_{\mathrm{c}y})T_{\mathrm{s}}]\boldsymbol{j}. \tag{40}$$

7) According to Eq. (40), the position error compensation amount along X- and Y-axis can be respectively expressed as $P_{\mathrm{ec}x}$ and $P_{\mathrm{ec}y}$, i.e.,

$$P_{\mathrm{ec}x} = E_x - (V_{Px} + V_{\mathrm{c}x})T_{\mathrm{s}}, \tag{41}$$

$$P_{\mathrm{ec}y} = E_y - (V_{Py} + V_{\mathrm{c}y})T_{\mathrm{s}}. \tag{42}$$

Finally, the calculated position error compensation corresponding to each sampling period is input into the two-axis servo system with certain proportional gains, thus realizing the advance compensation of tracking error.

4.2 Integrated motion control structure

The integrated control strategy for contour error compensation consists of a cross-coupling controller and an improved PEC. The overall structure of the integrated motion control is shown in Fig. 10. Different from that shown in Fig. 5, in Fig. 10, two modules of PEC and feed rate regulator are added and combined to form an improved PEC (as shown by the dashed box in Fig. 10).

In Fig. 10, $P_{\mathrm{ec}x}$ and $P_{\mathrm{ec}y}$ represent the position error compensations along X- and Y-axis, respectively, which can be obtained by Eqs. (41) and (42); $K_{\mathrm{pc}x}$ and $K_{\mathrm{pc}y}$ are gain coefficients corresponding to $P_{\mathrm{ec}x}$ and $P_{\mathrm{ec}y}$ of X- and Y-axis, respectively; and F is the feed rate. It can be seen from Fig. 10 that the cross-coupling controller and the improved PEC work together to change the control input of the system. At this time, based on Eqs. (9) and (10), a position error compensation term is added, and the output control law of the biaxial motion control system can be expressed as

$$U_x = R_x + P_{\mathrm{ec}x}K_{\mathrm{pc}x} + U_{\mathrm{c}}C_x, \tag{43}$$

$$U_y = R_y + P_{\mathrm{ec}y}K_{\mathrm{pc}y} + U_{\mathrm{c}}C_y. \tag{44}$$

The system's control input is updated in every sampling period. By inputting U_x and U_y obtained in real time as the reference position command of the current time into the two-axis servo system, the simultaneous compensation of contour error and tracking error can be realized.

5 Experimental setup and results

5.1 Experimental setup

To demonstrate the effectiveness of the proposed integrated control strategy, some experiments were performed on a biaxial motion control system shown in Fig. 11. The test objects are Delta ASDA A2-E series high-order AC servo driver and ECMA series motor, the NURBS interpolation is implemented in the computer, and the actual position of each axis is obtained by sampling the photoelectric encoder signal of the motor. Then, according

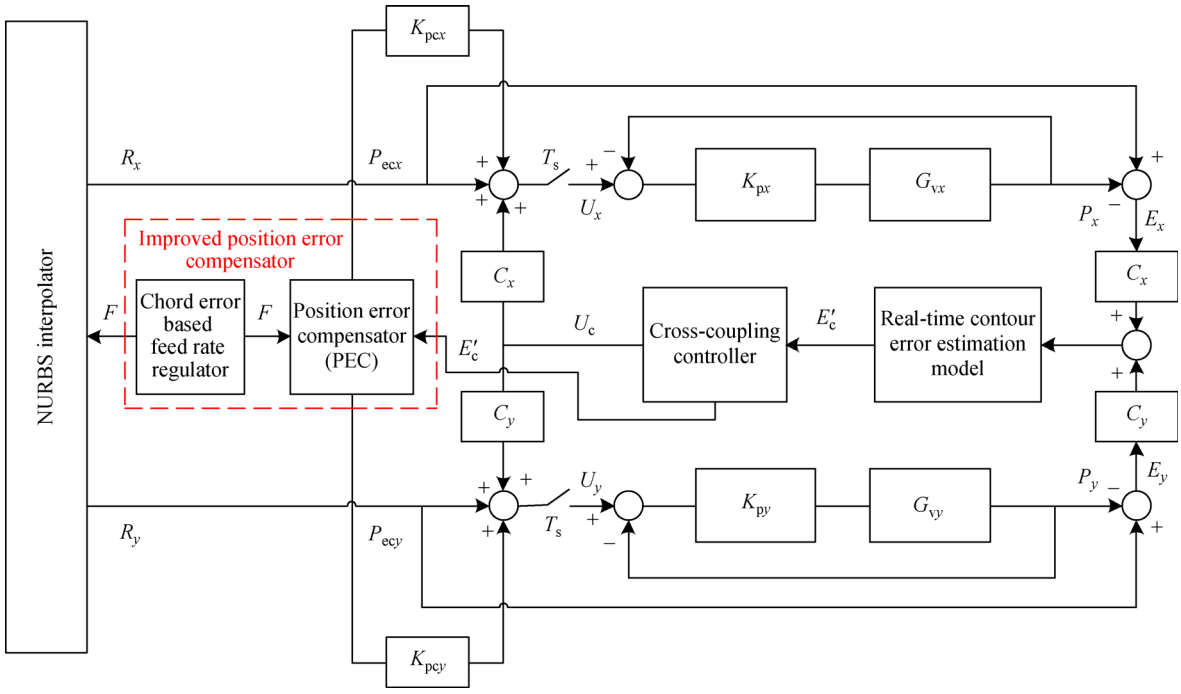

Fig. 10 Integrated motion control structure.

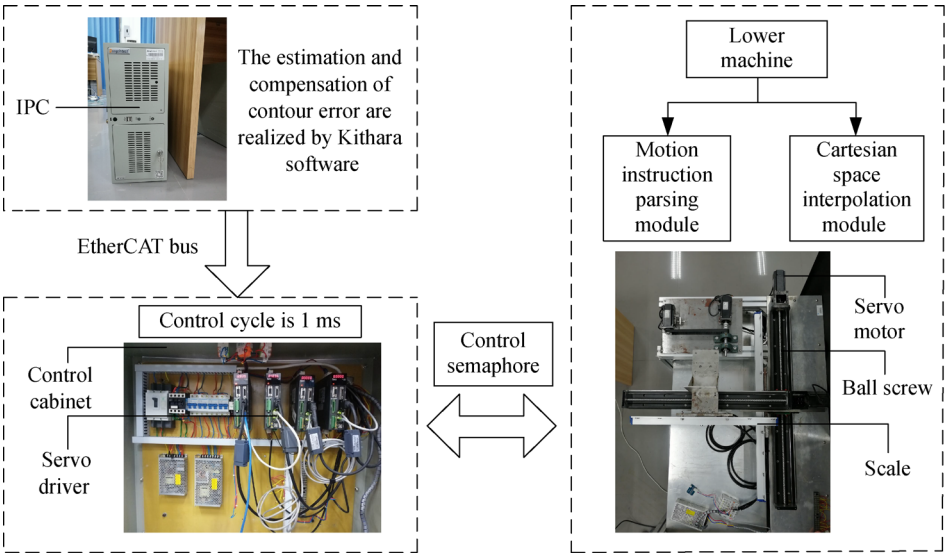

Fig. 11 Biaxial motion control system.

to the actual tracking curve and the ideal contour curve, the contour error can be calculated by using the real-time estimation algorithm of the contour error. The calculation and compensation of the real-time contour error are programmed on Kithara software, and the IPC sends the compensations to the servo unit via the EtherCAT bus. The system control cycle is set as $T_s = 1$ ms. In addition, the X–Y workbench consists of two ball screws (20 and 10 mm/r, respectively), and each ball screw is equipped with a grating with a resolution of 1 μm. The gain constants used in the experiment are: $K_{px} = 35$, $K_{py} = 35$, $K_{cp} = 2.0$, $K_{ci} = 0.001$, $K_{pcx} = 1.0$, and $K_{pcy} = 1.0$. The maximum allowable chord error is set as 0.001 mm.

5.2 Experimental results

Multiple groups of comparison experiments were performed for two different target trajectories respectively named “star curve” (as shown in Fig. 12(a)) and “free curve” (as shown in Fig. 12(b)). For the “star curve”, the

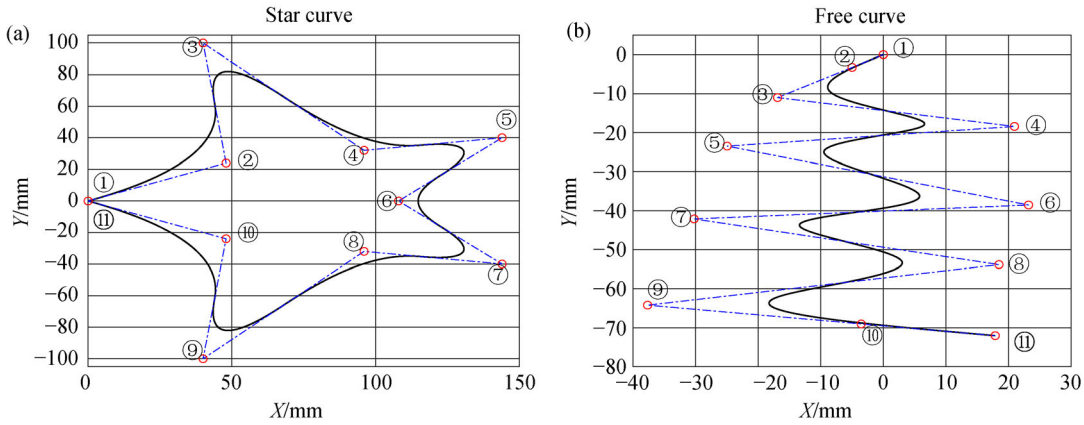

Fig. 12 Reference paths in the contour following tasks: Reference path of (a) the "star curve" and (b) the "free curve".

minimum radius of curvature is 3.5 mm, and for the "free curve", the minimum radius of curvature is 0.5 mm. The reference position commands for both trajectories are generated by the NURBS curve interpolator, and the curve parameters are listed in Table 2. For the "star curve", the order is $k = 2$ and the knot vector is (0, 0, 0, 1/9, 2/9, 3/9, 4/9, 5/9, 6/9, 7/9, 8/9, 1, 1, 1). For the "free curve", the order is $k = 3$ and the knot vector is (0, 0, 0, 0, 0.0776395399490, 0.1853424960819, 0.2923660845951, 0.4098664482764, 0.5360574750026, 0.6509686913241, 0.7809426259331, 1, 1, 1, 1). The comparison schemes of the experiments are as follows: 1) Comparing the experimental results of three position-loop control schemes under constant feed rate condition; 2) comparing the experimental results of the CCC + PEC control scheme and the integrated control strategy. Note that the parameter u in Figs. 13–17 of the experimental results refers to the parameter of the NURBS curve, which has been described in Section 2.

5.2.1 Analysis of contour following experimental results under constant feed rate

In this experiment, each contour following task was completed and tested using three position loop control schemes, namely without contour error compensation (i.e., none CCC method), compensating for contour error using a PI-type cross-coupling controller (i.e., CCC method) and a PEC based on CCC (i.e., CCC + PEC method).

5.2.1.1 Analysis of the experimental results for the "star curve"

The contour and tracking errors of the "star curve" are shown in Fig. 13. The contour following task is completed under the condition of constant feed rate (200 mm/s). Figures 13(a)–13(c) respectively show the absolute contour errors estimated in real time using the three above-mentioned control schemes. Figures 13(d) and 13(e) show

Table 2 Parameters of the "star curve" and the "free curve"

Vertex number	Parameters of the "star curve"		Parameters of the "free curve"	
	Control point coordinate/mm	Weight	Control point coordinate/mm	Weight
1	(0, 0)	1.0	(0, 0)	1.0
2	(48, 24)	1.0	(–4.99420, –3.24613)	1.0
3	(40, 100)	1.0	(–16.91645, –10.99536)	1.0
4	(96, 32)	1.0	(20.95161, –18.41546)	1.0
5	(144, 40)	0.7	(–24.97704, –23.46105)	1.0
6	(108, 0)	1.0	(23.20926, –38.53194)	1.0
7	(144, –40)	0.7	(–30.24880, –42.11590)	1.0
8	(96, –32)	1.0	(18.47811, –53.82904)	1.0
9	(40, –100)	1.0	(–37.67975, –64.20412)	1.0
10	(48, –24)	1.0	(–3.54279, –69.02725)	1.0
11	(0, 0)	1.0	(17.88210, –72.05432)	1.0

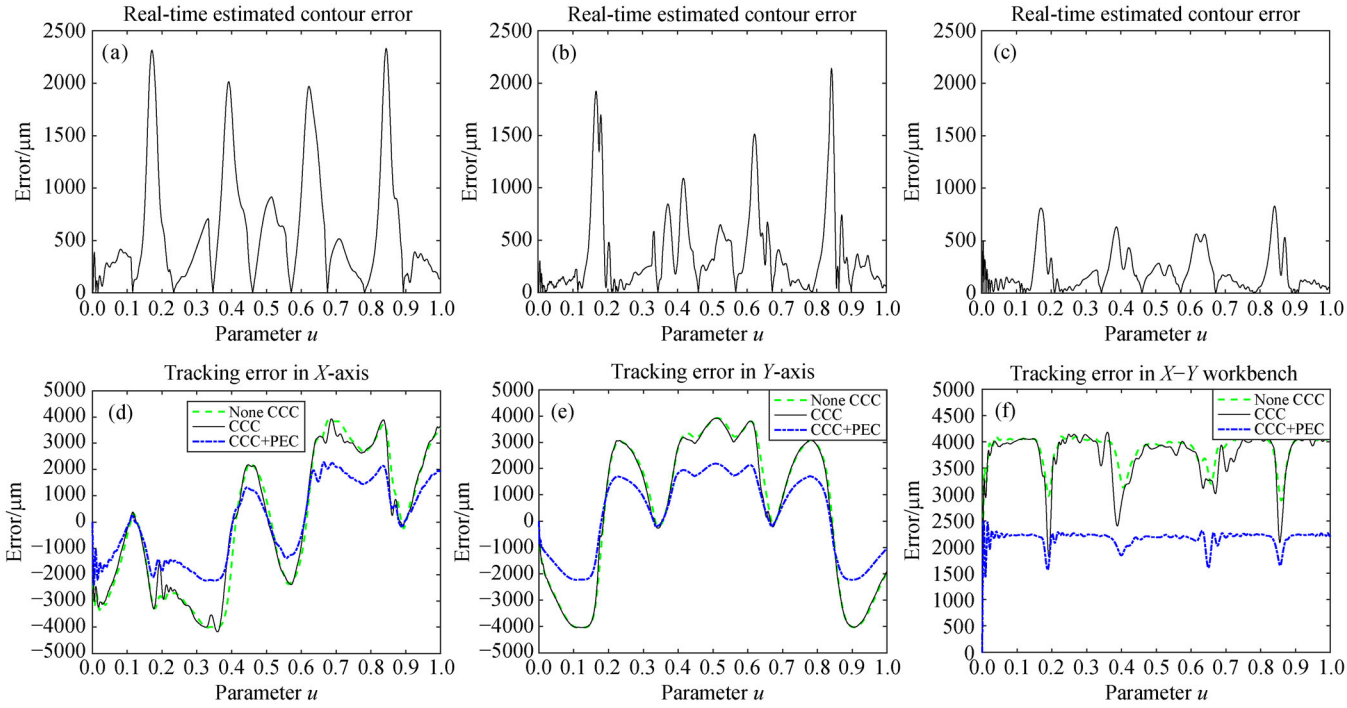

Fig. 13 Comparison of the experimental results of contour and tracking errors for the "star curve": Contour error (a) without CCC, (b) with CCC, and (c) with CCC + PEC; tracking error in (d) *X*- and (e) *Y*-axis, respectively, and (f) *X*–*Y* workbench.

the experimental results of tracking error respectively in *X*- and *Y*-axis obtained by the three control schemes, and Fig. 13(f) shows the experimental results of the tracking error in *X*–*Y* workbench obtained by the three control schemes. From the experimental results shown in Table 3, it can be seen that, as compared with the case without CCC, CCC scheme helps to reduce the root mean square contour error by 34.8%, while the root mean square tracking error hardly changes. Moreover, it is found that CCC + PEC scheme helps to reduce the root mean square contour error by 67.2%, with the root mean square tracking error being also reduced by 44.2%.

5.2.1.2 Analysis of the experimental results for the "free curve"

The contour and tracking errors of the "free curve" are shown in Fig. 14 and the contour following task is completed under the condition of constant feed rate (100 mm/s). Figures 14(a)–14(c) respectively show the absolute contour errors estimated in real time using the three above-mentioned control schemes. Figures 14(d) and 14(e) show the experimental results of tracking error respectively in *X*- and *Y*-axis obtained by the three control schemes, and Fig. 14(f) shows the experimental results of the tracking error in *X*–*Y* workbench obtained by the three control schemes. From the experimental results shown in Table 3, it can be seen that, as compared with the case without CCC, CCC scheme helps to reduce the root mean square contour error by 44.0%, while the root mean square tracking error hardly changes. Moreover, it is found that CCC + PEC scheme helps to reduce the root mean square contour error by 65.4%, with the root mean square tracking error being also reduced by 42.6%.

Table 3 Experimental results obtained by the three control schemes under constant feed rate

Experimental subject	Experimental condition	Performance index of tracking error/μm		Performance index of contour error/μm	
		$\|\|M\|\|_{max}$	RMS	$\|\|M\|\|_{max}$	RMS
"Star curve" (with constant feed rate: 200 mm/s)	None CCC	4109.50	3913.40	2329.70	642.43
	CCC	4205.70	3822.30	2139.10	419.07
	CCC + PEC	2496.70	2184.80	828.72	210.96
"Free curve" (with constant feed rate: 100 mm/s)	None CCC	2227.10	1866.80	1572.20	414.34
	CCC	2188.90	1831.80	1163.20	231.94
	CCC + PEC	1383.40	1070.80	662.51	143.48

Note: $\|\|M\|\|_{max}$ represents the maximum error, and RMS represents the root mean square error.

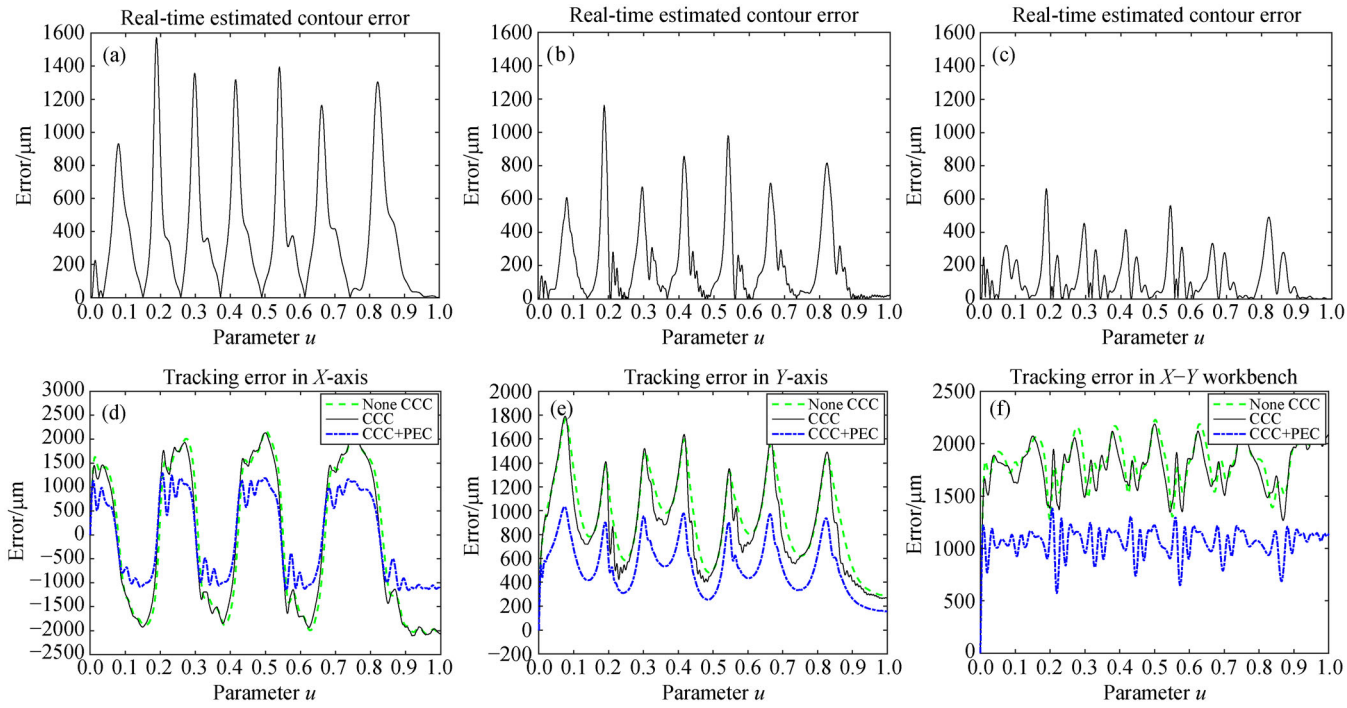

Fig. 14 Comparison of the experimental results of contour and tracking errors for the "free curve": Contour error (a) without CCC, (b) with CCC, and (c) with CCC + PEC; tracking error in (d) *X*-, and (e) *Y*-axis, respectively, and (f) *X*–*Y* workbench.

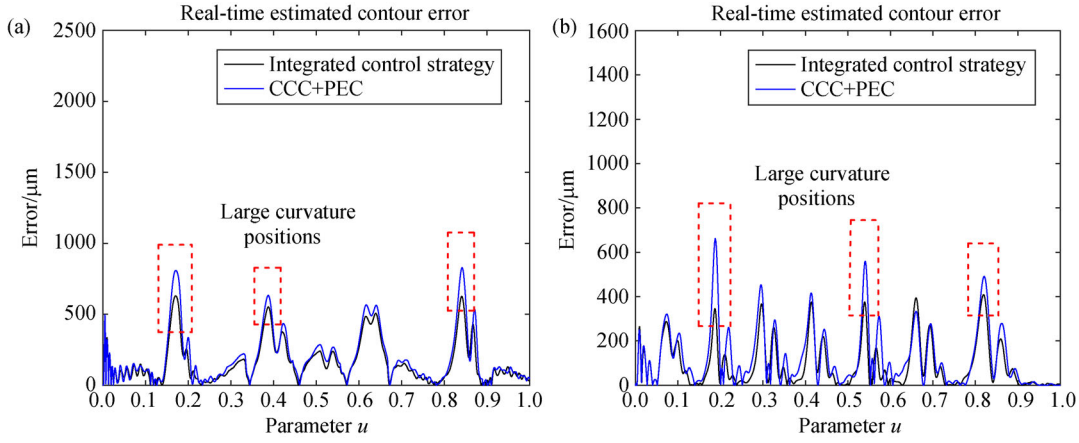

Fig. 15 Comparison of contour error results for (a) the "star curve" and (b) the "free curve".

5.2.2 Analysis of the experiment results of contour following obtained by the integrated control strategy

To verify the effectiveness of the proposed integrated control strategy, the experimental results obtained by the CCC + PEC control scheme are compared with those of the contour error test obtained by the integrated control strategy. Figures 15(a) and 15(b) show the experimental results of real-time estimated absolute contour error obtained by two control schemes respectively for the "star curve" and the "free curve", and the corresponding performance indexes of contour error are listed in Table 4. Figures 16(a) and 16(b) show the variation laws of feed rate, acceleration and jerk after the planning for the "star curve" and the "free curve", respectively. Figures 17(a) and 17(b) show the distribution curves of chord errors for the "star curve" and the "free curve", respectively. It can be seen from Fig. 17 that the chord errors of the two target trajectories are within the range of the maximum allowed chord error. The experimental results listed in Table 4 indicate that, with the adoption of the integrated control strategy for the "star curve", the maximum value of the contour error reduces by 24.0%, as compared with that obtained by the CCC + PEC control scheme, and the root mean square contour error reduces by 17.1%. Moreover, for the "free curve" adopting the integrated control

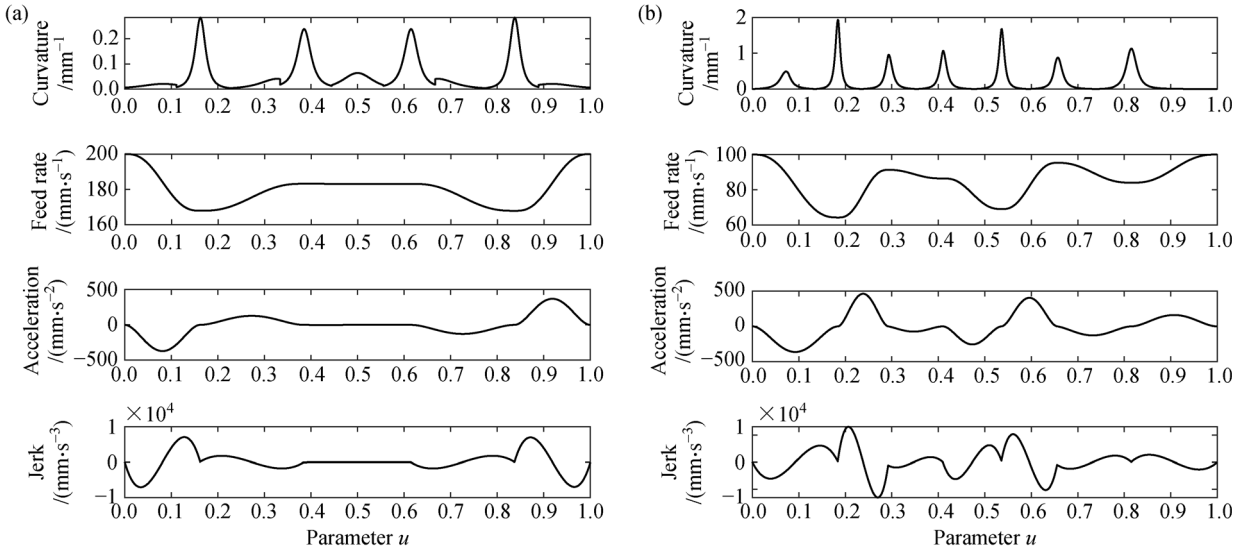

Fig. 16 Variation laws of feed rate, acceleration and jerk after the planning: Variation laws for (a) the "star curve" and (b) the "free curve".

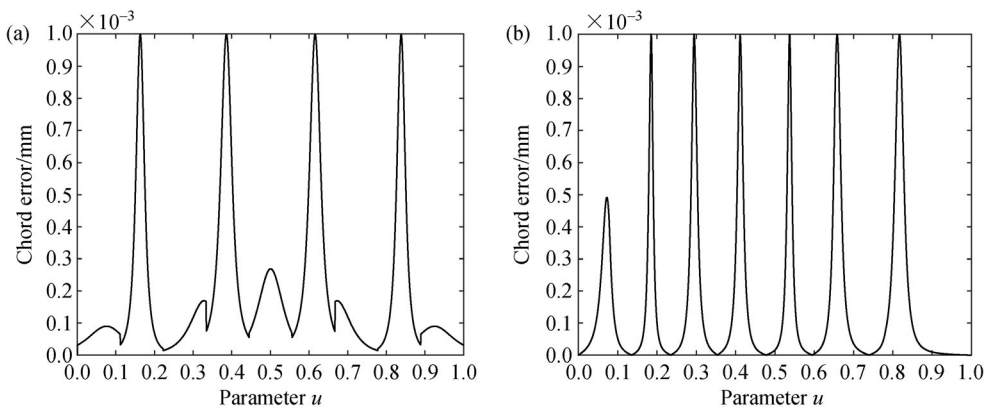

Fig. 17 Distribution curves of chord errors for (a) the "star curve" and (b) the "free curve".

Table 4 Performance indexes of contour error obtained by the CCC + PEC control scheme and the integrated control strategy

Experimental condition	Performance index of contour error for the "star curve"/μm		Performance index of contour error for the "free curve"/μm	
	$\|M\|_{\max}$	RMS	$\|M\|_{\max}$	RMS
CCC + PEC control scheme	828.72	210.96	662.51	143.38
Integrated control strategy	629.72	174.88	408.35	109.58

strategy, the maximum value of the contour error reduces by 38.4%, as compared with that obtained by the CCC + PEC control scheme, and the root mean square contour error reduces by 23.6%. All these mean that the proposed integrated control strategy not only satisfies the requirements for the chord error in the machining process, ensures the continuity of acceleration and jerk, but also further reduces the contour error in large curvature positions (as shown by the dashed box in Fig. 15) with the help of the CCC + PEC control scheme.

6 Conclusions

1) To solve the problem that the traditional CCC method cannot meet the chord error requirement in large curvature positions, a feed rate regulator based on the chord error constraint is proposed.

2) Based on the improved CCC structure, a PI-type cross-coupling controller is designed, with its stability being analyzed by using the CETF.

3) An integrated control strategy for cross-coupling

contour error compensation based on chord error constraint is also proposed, which consists of a cross-coupling controller and an improved PEC.

4) Biaxial contour control experiments were carried out using NURBS curves. The results show that the CCC + PEC control scheme improves the tracking accuracy and contour control accuracy of the curve at the same time, and that the proposed integrated control strategy helps to obtain higher contour control accuracy than the CCC + PEC control scheme.

Acknowledgements This work was supported by the National Science and Technology Major Project of China (Grant No. 2015ZX04005006), and the Science and Technology Major Project of Zhongshan City, China (Grant Nos. 2016F2FC0006 and 2018A10018).

References

1. Koren Y. Cross-coupled biaxial computer control for manufacturing systems. Journal of Dynamic Systems, Measurement, and Control, 1980, 102(4): 265–272
2. Koren Y, Lo C C. Variable-gain cross-coupling controller for contouring. CIRP Annals, 1991, 40(1): 371–374
3. Zhao H, Zhu L M, Ding H. Cross-coupled controller based on high-precision contouring error estimation. Journal of Mechanical Engineering, 2014, 50(3): 158–164 (in Chinese)
4. Wu J, Liu C, Xiong Z, et al. Precise contour following for biaxial systems via an A-type iterative learning cross-coupled control algorithm. International Journal of Machine Tools and Manufacture, 2015, 93: 10–18
5. Su K H, Cheng M Y. Contouring accuracy improvement using cross-coupled control and position error compensator. International Journal of Machine Tools and Manufacture, 2008, 48(12–13): 1444–1453
6. Yang J, Li Z. A novel contour error estimation for position loop-based cross-coupled control. IEEE/ASME Transactions on Mechatronics, 2011, 16(4): 643–655
7. Shih Y T, Chen C S, Lee A C. A novel cross-coupling control design for bi-axis motion. International Journal of Machine Tools and Manufacture, 2002, 42(14): 1539–1548
8. Chen H R, Cheng M Y, Wu C H, et al. Real time parameter based contour error estimation algorithms for free form contour following. International Journal of Machine Tools and Manufacture, 2016, 102: 1–8
9. Yan M T, Lee M H, Yen P L. Theory and application of a combined self-tuning adaptive control and cross-coupling control in a retrofit milling machine. Mechatronics, 2005, 15(2): 193–211
10. Chen W, Wang D, Geng Q, et al. Robust adaptive cross-coupling position control of biaxial motion system. Science China. Technological Sciences, 2016, 59(4): 680–688
11. Srinivasan K, Kulkarni P K. Cross-coupled control of biaxial feed drive servomechanisms. Journal of Dynamic Systems, Measurement, and Control, 1990, 112(2): 225–232
12. Ouyang P R, Dam T, Pano V. Cross-coupled PID control in position domain for contour tracking. Robotica, 2015, 33(6): 1351–1374
13. Chen C S, Chen L Y. Cross-coupling position command shaping control in a multi-axis motion system. Mechatronics, 2011, 21(3): 625–632
14. Sun W, Zhang Y, Huang Y, et al. Transient-performance-guaranteed robust adaptive control and its application to precision motion control systems. IEEE Transactions on Industrial Electronics, 2016, 63(10): 6510–6518
15. El Khalick M A, Uchiyama N. Discrete-time model predictive contouring control for biaxial feed drive systems and experimental verification. Mechatronics, 2011, 21(6): 918–926
16. Wu J, Han Y, Xiong Z, et al. Servo performance improvement through iterative tuning feedforward controller with disturbance compensator. International Journal of Machine Tools and Manufacture, 2017, 117: 1–10
17. Cheng M Y, Su K H, Wang S F. Contour error reduction for free-form contour following tasks of biaxial motion control systems. Robotics and Computer-Integrated Manufacturing, 2009, 25(2): 323–333
18. Chen C S, Fan Y H, Tseng S P. Position command shaping control in a retrofitted milling machine. International Journal of Machine Tools and Manufacture, 2006, 46(3–4): 293–303
19. Moghadam H Z, Landers R G, Balakrishnan S N. Hierarchical optimal contour control of motion systems. Mechatronics, 2014, 24(2): 98–107
20. Tang L, Landers R G. Predictive contour control with adaptive feed rate. IEEE/ASME Transactions on Mechatronics, 2012, 17(14): 669–679
21. Rahaman M, Seethaler R, Yellowley I. A new approach to contour error control in high speed machining. International Journal of Machine Tools and Manufacture, 2015, 88: 42–50
22. Barton K L, Alleyne A G. A cross-coupled iterative learning control design for precision motion control. IEEE Transactions on Control Systems Technology, 2008, 16(6): 1218–1231
23. Tsai M S, Yen C L, Yau H T. Iterative learning control based on a hybrid tracking and contour error algorithm. In: Proceedings of 2009 IEEE/ASME International Conference on Advanced Intelligent Mechatronics. Singapore: IEEE, 2009, 650–655
24. Song D N, Zhong Y G, Ma J W. Third-order contour-error estimation for arbitrary free-form paths in contour-following tasks. Precision Engineering, 2019, 60: 85–92
25. Yang J, Ding H, Zhao H, et al. A generalized on-line estimation and control of five-axis contouring errors of CNC machine tools. International Journal of Machine Tools and Manufacture, 2015, 88: 9–23
26. Yang J, Ding H, Zhao H, et al. A generalized online estimation algorithm of multi-axis contouring errors for CNC machine tools with rotary axes. International Journal of Advanced Manufacturing Technology, 2016, 84(5–8): 1239–1251
27. Cheng M Y, Tsai M C, Kuo J C. Real-time NURBS command generators for CNC servo controllers. International Journal of Machine Tools and Manufacture, 2002, 42(7): 801–813
28. Yeh S S, Hsu P L. Theory and applications of the robust cross-coupled control design. In: Proceedings of the 1997 American Control Conference. Albuquerque: IEEE, 1997